# Occurrence of Hydrothermal Alteration Minerals at the Jade Hydrothermal Field, in the Izena Hole, Mid-Okinawa Trough

44

Youko Miyoshi, Jun-ichiro Ishibashi, Kazuhiko Shimada, Mitsuhiro Ooki, Seiichiro Uehara, Ryoto Yoshizumi, Shota Watanabe, and Tetsuro Urabe

**Abstract**

Mineralogical and geochemical features of hydrothermal alteration minerals in the sediment cores from the Jade hydrothermal field in the Izena Hole, mid-Okinawa Trough, were studied by XRD, EPMA and TEM-EDS analyses. A core sample 1186MBL collected from the surface sediment near the sulfide chimney venting high temperature fluid up to 320 °C was characterized by occurrence of kaolinite, with sulfide minerals such as sphalerite and galena. The kaolinite would be related to be formed under acidic condition caused by oxidation and dissolution of the sulfide minerals by penetrating seawater. Core samples (1188MB, 1193MB) were collected from the surface sediment in the vicinity of clear hydrothermal fluid venting of ~100 °C, which is located in 400 m distant from the sulfide chimney. In these cores, occurrence of chlorite and smectite was identified. The chlorite in the core 1188MB had chemical composition close to Al-rich chlorite which is classified as sudoite, although chlorite found in other hydrothermal fields in the Okinawa Trough is characterized as significantly Mg-rich chlorite. Core samples of up to 4–6 m length were also collected near the low temperature fluid venting to study alteration in deep layers. One of two long core samples (BMS-J-2) was characterized by chlorite and illite assemblage below 380 cmbsf, while the other (LC-J-2) was characterized by abundant occurrence of K-feldspar below 300 cmbsf. Occurrence of euhedral crystals of K-feldspar in size up to several tens μm suggests the formation by precipitation from high temperature fluid.

**Keywords**

Clay mineral • Electron probe micro-analyzer (EPMA) • Okinawa Trough • Transmission electron microscope (TEM-EDS) • X-ray diffraction (XRD)

The online version of this chapter (doi:10.1007/978-4-431-54865-2_44) contains supplementary material, which is available to authorized users.

Y. Miyoshi (✉)
Graduate School of Sciences, Kyushu University, 6-10-1 Hakozaki, Higashi-ku, Fukuoka 812-8581, Japan

Present address: Institute for Geo-Resources and Environment, National institute of Advanced Industrial Science and Technology (AIST), Central-7, 1-1-1 Higashi, Tsukuba, Ibaraki 305-8567, Japan
e-mail: youko-miyoshi@aist.go.jp

J.-i. Ishibashi • K. Shimada • M. Ooki • S. Uehara
Graduate School of Sciences, Kyushu University, 6-10-1 Hakozaki, Higashi-ku, Fukuoka 812-8581, Japan

R. Yoshizumi • T. Urabe
Graduate School of Science, The University of Tokyo, 7-3-1 Hongo, Bunkyo-ku, Tokyo 113-0033, Japan

S. Watanabe
Graduate School of Life and Environmental Sciences, University of Tsukuba, 1-1-1 Ten-noudai, Tsukuba, Ibaraki 305-8572, Japan

J.-i. Ishibashi et al. (eds.), *Subseafloor Biosphere Linked to Hydrothermal Systems: TAIGA Concept*,
DOI 10.1007/978-4-431-54865-2_44, 

## 44.1 Introduction

Most of active hydrothermal fields in the Okinawa Trough are located in sediment-rich environment (Ishibashi et al., Chap. 29), where extensive hydrothermal alteration is expected to occur as a result of subseafloor fluid-sediment interactions. Marumo and Hattori (1999) documented occurrence of diverse hydrothermal alteration minerals in sediment collected from the Jade field in the mid-Okinawa Trough. Miyoshi (2013) studied geochemical and mineralogical features of hydrothermal alteration minerals in sediment cores obtained by drilling during IODP (Integrated Ocean Drilling Program) Expedition 331 at the Iheya North Knoll field in the mid-Okinawa Trough (Takai et al., 2011). Results of this study suggested layered structure of distinctive alteration zones consisted of various clay minerals.

In this chapter, we report results of mineralogical and geochemical analyses of hydrothermal alteration minerals in sediment collected from the Jade field of the Izena Hole, in the mid-Okinawa Trough (Fig. 44.1a). Recent dive studies documented two different types of hydrothermal fluid venting in the Jade field (Ishibashi et al., 2014). While vigorous venting of high temperature fluid up to 320 °C from sulfide chimneys is observed at water depth of ~1,350 m, diffusive venting of clear hydrothermal fluid of ~100 °C is located at water depth of ~1,550 m. A geochemical study revealed distinctive fluid chemistry between the high temperature fluid and low temperature fluid (Ishibashi et al., 2014). Since mineralogy of hydrothermal alteration minerals reflects physical and chemical conditions of their formation, different types of hydrothermal mineralogy is expected to be identified in sediment collected from the seafloor around these two vent sites. And comparison of their mineralogy would provide important clues to discuss chemical environment within sediment near active vent sites.

## 44.2 Geological Background

The Jade field is located on a slope of a north-eastern wall of the Izena Hole (Fig. 44.1a). Hydrothermal activity was recognized in an area of 500 m × 300 m at water depth between 1,300 and 1,550 m (Fig. 44.1b). At water depth of ~1,350 m, vigorous venting of high temperature fluid from sulfide chimneys and spires was recognized (Sakai et al., 1990a). A tall sulfide chimney venting the highest temperature fluid in Jade site (=320 °C) was named as Black Smoker Chimney (or TBS Chimney). Active and inactive chimneys are likely to align along NE–SW direction on the slope. At ~150 m northeast from the Black Smoker Chimney, an active sulfide chimney venting clear fluid of 60–70 °C is recognized at water depth of ~1,320 m, which was called as Red Star Chimney. At extension of the alignment in the southwest direction at water depth of ~1,500 m, diffusive venting of clear hydrothermal fluid from a small depression on the seafloor was located, which was called as Biwako Vent (Ishibashi et al., 2014). Temperature of the Biwako Vent fluid was 90 ~ 104 °C. Around the Biwako Vent, emanation of liquid $CO_2$ bubble was observed in several sites, one of which was reported in Sakai et al. (1990b). Extensive distribution of consolidated sediment containing amorphous silica and native sulfur was recognized also in the vicinity of the Biwako Vent, which was called as Sulfur Reef site.

A previous study documented distinctive fluid chemistry between these venting fluids (Ishibashi et al., 2014). High temperature fluid venting from the Black Smoker Chimney showed slightly higher Cl concentration than that of seawater. And fluid temperature of 320 °C is close to the boiling point at the seafloor depth. Based on the physical and chemical property, the Black Smoker Chimney fluid is considered the mainstream of focused upflow that has undergone slight loss of the vapor phase after the subseafloor phase separation (Ishibashi et al., 2014). Chemical composition of low temperature fluid obtained from the Red Star Chimney was explained by mixing between the hydrothermal component shared with the Black Smoker Chimney fluid and seawater, prior to venting from the seafloor. On the other hand, low temperature fluid venting from the Biwako Vent showed significantly low Cl concentration that is about one thirds of seawater level. Together with notably high $H_2S$ concentration, fluid chemistry of the Biwako Vent is attributed to be originated from the vapor phase segregated during subseafloor phase separation.

Different features between these two areas are notable not only in fluid chemistry but also in appearance of the seafloor surrounding the vent sites (Ishibashi et al., 2014). Abundant sulfide breccia and particles likely formed by collapse of inactive chimneys are recognized on the seafloor around the Black Smoker Chimney and the Red Star Chimney. Contrarily, white patches in sediment implying hydrothermal alteration are notable as well as consolidated sediment crusts on the seafloor in the area around the Biwako Vent. Other than hydrothermal active areas, most part of the seafloor in the Jade field is covered with tuff breccia and woody pumice.

## 44.3 Materials and Method

### 44.3.1 Sample Collection

Sediment cores were collected by an acrylic push corer (MBARI-type corer) attached to remotely operated vehicle (ROV) Hyper-Dolphin, which aimed to collect surface sediment up to ~30 cmbsf (centimeters below the seafloor)

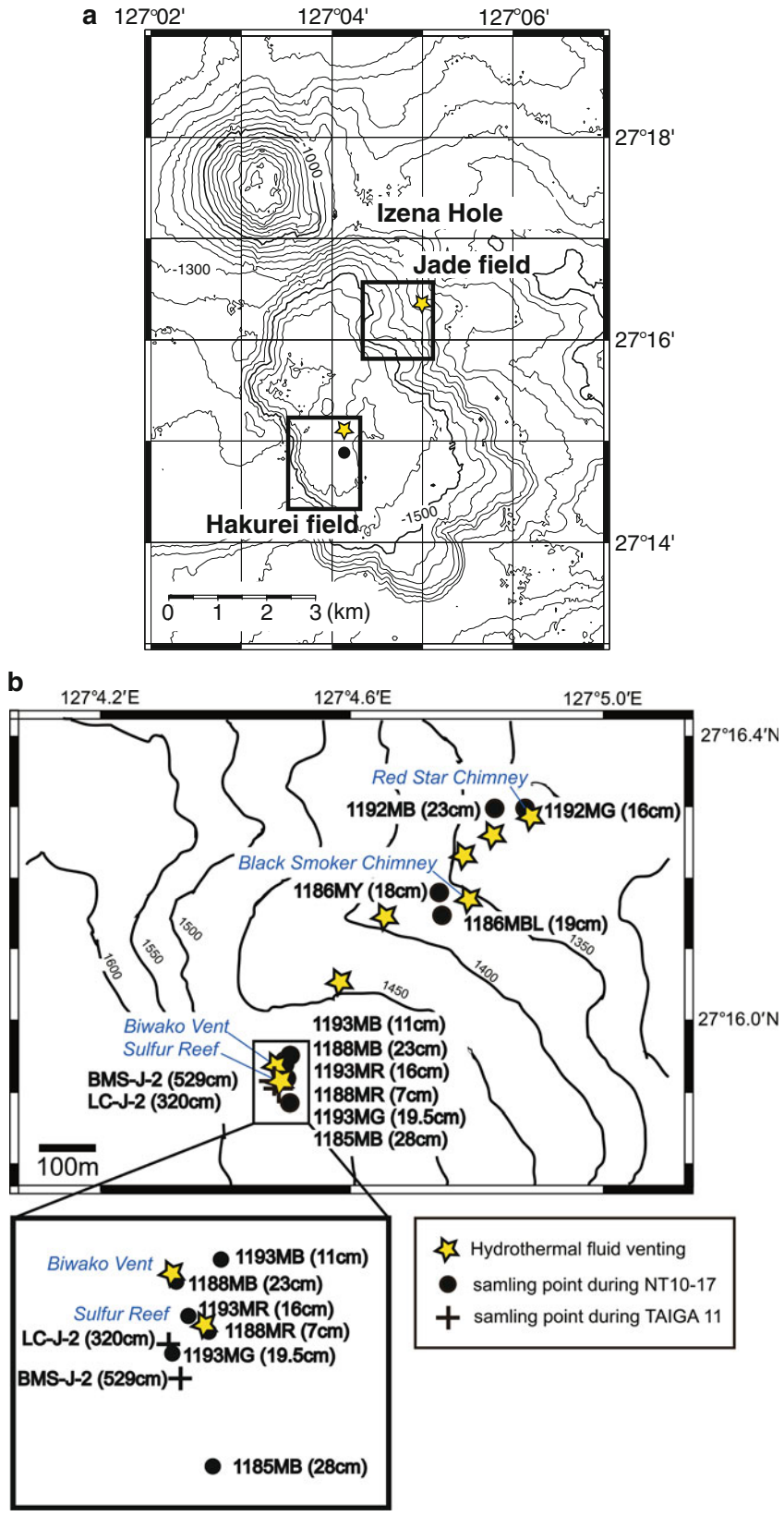


**Fig. 44.1** Bathymetric map of (**a**) the Izena Hole and (**b**) Jade field. The upper *box* in (**a**) indicates area shown in (**b**). The *yellow star marks* represent active hydrothermal vent. The *closed circles* and *cross marks* represent the localities of short cores during the NT10-17 cruise, and of long cores during the TAIGA11 cruise

**Table 44.1** List of sediment core samples for this study, collected during the NT10-17 cruise and TAIGA11 cruise

| Core ID | Latitude | Longitude | Depth (m) | Sampling location |
|---|---|---|---|---|
| NT10-17 | | | | |
| 1185MB | 27° 15.885′ N | 127° 4.503′ E | 1,554 | ~50 m south of the Sulfur Reef site |
| 1186MY | 27° 16.182′ N | 127° 4.741′ E | 1,357 | ~50 m west of the Black Smoker Chimney |
| 1186MBL[a] | 27° 16.150′ N | 127° 4.745′ E | 1,376 | ~50 m southwest of the Black Smoker Chimney |
| 1187MB | 27° 14.928′ N | 127° 4.148′ E | 1,603 | ~30 m south of the Dragon Chimney in the Hakurei field |
| 1188MR | 27° 15.928′ N | 127° 4.502′ E | 1,523 | At the Sulfur Reef |
| 1188MB[a] | 27° 15.944′ N | 127° 4.494′ E | 1,520 | Adjacent to the Biwako Vent |
| 1192MB | 27° 16.299′ N | 127° 4.829′ E | 1,312 | ~50 m west of the Red Star Chimney |
| 1192MG | 27° 16.299′ N | 127° 4.877′ E | 1,306 | A few meters distant from the Red Star Chimney (1) |
| 1193MG | 27° 15.921′ N | 127° 4.493′ E | 1,543 | At the Sulfur Reef (2) |
| 1193MR | 27° 15.933′ N | 127° 4.497′ E | 1,537 | At the Sulfur Reef (3) |
| 1193MB[a] | 27° 15.951′ N | 127° 4.505′ E | 1,521 | Adjacent to the $CO_2$ bubbling site (4) |
| TAIGA11 | | | | |
| BMS-J-2[a] | 27° 15.913′ N | 127° 4.495′ E | 1,520 | ~80 m south of the Biwako Vent |
| LC-J-2[a] | 27° 15.924′ N | 127° 4.492′ E | 1,570 | Near the Biwako Vent (5) |

[a]These cores were examined in detail by this study, because hydrothermally altered mud was observed in these cores
(1) Native sulfur filling fissures in the sediment was observed
(2) Core sampling was attempted to collect consolidated sediment, but only overlaying sediment was collected
(3) Core sampling was attempted after the consolidated sediment crust was broken by a manupilator
(4) When the corer pulled out, liquid $CO_2$ bubble was emanated from the seafloor
(5) The sampling locality was determined by navigation of the surface ship

without any disturbance. Hereafter, this type of core is called as a short core. Short core sampling was conducted during the NT10-17 cruise of R/V Natsushima (Japan Agency for Marine-Earth Science and Technology (JAMSTEC)) in September 2010. In total 11 short cores were collected during the cruise, as summarized in Table 44.1. Sampling localities are shown with bathymetric maps in Fig. 44.1b. Two short cores (1186MBL and 1186MY) were collected near the Black Smoker Chimney, two short cores (1192MB and 1192MG) near the Red Star Chimney, six short cores (1185MB, 1188MR, 1188MB, 1193MR, 1193MG and 1193MB) around the Sulfur Reef and Biwako Vent. One additional short core (1187MB) was collected from the seafloor near the Dragon Chimney in the Hakurei field, which is located at ~3 km southwest of the Jade filed and on the basin seafloor of the Izena Hole (Fig. 44.1a).

Another type of coring operation was conducted using a Benthic Multi-coring System (BMS) and a large-diameter gravity corer (LC). As described in Ishibashi et al. (Chap. 31), these coring apparatus enabled us to collect sediment from the surface to 4–6 mbsf (meters below the seafloor), although the sampling sometimes suffered from poor recovery. Hereafter, this type of core is called as a long core. Coring operations with a BMS and LC were conducted during the TAIGA11 cruise of the R/V Hakurei-Maru No. 2 (Japan Oil, Gas and Metals National Corporation (JOGMEC)) in May to June 2011 (Ishibashi et al., Chap. 31). In the Jade field, coring was attempted at four stations (BMS-J-2, BMS-J-3A, BMS-J-3B, and LC-J-2). In this study, the core samples from BMS-J-2 and LC-J-2 were studied because of their good recovery.

### 44.3.2 Sample Analysis

Sediment subsamples were collected from the obtained cores at 5 to 10 cm intervals. During the expeditions, they were refrigerated. After return to the laboratory, some of the sediment samples were disaggregated in distilled water. After they settled out, they were disaggregated in new distilled water again. The work was repeated several times to remove dissolved salts. Clay fractions (<2 μm) were collected from suspending particles in the distilled water after leaving 5 hours according to the Stokes' law.

Minerals in the sediment samples obtained by NT10-17 expedition were identified by X-ray diffraction (XRD), Rigaku RAD II A, at the Department of Earth and Planetary Sciences, Kyushu University. The XRD was conducted at 30 kV and 15 mA using Ni-filtered Cu-Kα ($\lambda = 1.5418$ Å) radiation. Step scan XRD data (2–64° 2θ, 0.05° 2θ step width, 1.0 s/step) were collected for bulk sediment samples. Step-scan XRD data (2–32° 2θ, 0.05° 2θ step width, 1.0 s/step) were collected for clay fraction samples, under air-dried, ethylene glycol-saturated and HCl treated conditions. Minerals in the sediment samples obtained by TAIGA 11 expedition were identified by X-ray diffraction (XRD), M18XHF22-SRA, MXP18 (BRUKER axs), at the Department of Earth and Planetary Sciences, Kyushu University. The XRD was conducted at 40 kV and 100 or 50 mA using Ni-filtered Cu-Kα ($\lambda = 1.54056$ Å) radiation. Step scan XRD data (2–64° 2θ, 0.05° 2θ step width, 0.5 or 1.0 s/step) were collected for bulk sediment samples. Step-scan XRD data (2–32° 2θ, 0.05° 2θ step width, 0.5 or

**Table 44.2** Visual core descriptions of the short core samples, (a) 1186MBL, (b) 1188MB, and (c) 1193MB

| Core ID | Core length (cm) | Depth (cmbsf) | Visual description of the core |
|---|---|---|---|
| (a) | | | |
| 1186MBL | 19 | 0–2 | |
| | | 2–4 | Pumice |
| | | 4–9 | Sulfur grains, sulfide grains, pumice |
| | | 9–15 | Sulfur grains, pumice |
| | | 15–17 | |
| | | 17–19 | Sulfur lump of pipe-like shape |
| (b) | | | |
| 1188MB | 23 | 0–2 | Upper layer: unaltered sand sediment<br>Lower layer: white gray colored hydrothermal altered mud |
| | | 2–23 | White gray colored hydrothermal altered mud |
| (c) | | | |
| 1193MB | 11 | 0–4 | |
| | | 4–7 | Pumice |
| | | 7–9 | Whitish mud, sulfur grains |
| | | 9–11 | Whitish mud, sulfur grains |

1.0 s/step) were collected for clay fraction samples, under air-dried and ethylene glycol-saturated conditions.

Morphology and chemical composition of clay mineral particles were determined using a transmission electron microscope (TEM) equipped with an energy dispersive spectrometer (EDS), JEOL JEM-2010FEF, in the Research Laboratory for High Voltage Electron Microscopy (HVEM), Kyushu University. The TEM (JEOL JEM-2010FEF) was operated at an accelerating voltage of 200 kV. Samples for TEM-EDS analysis were prepared by settling on a carbon-coated copper grid after ultrasonic dispersion of powdered clay fractions in alcohol. To analyze chemical composition, clay mineral particles without overlapping were selected under the TEM observation.

Sediment samples were observed and analyzed using an electron probe micro-analyzer (EPMA), JEOL JXA-8530F, at the Department of Earth and Planetary Sciences, Kyushu University. Determination of chemical composition of minerals in the samples was done by a wavelength dispersive spectrometer (WDS) attached to the EPMA. For this measurement, the samples were fixed with resin onto a thin section and polished.

## 44.4 Results and Discussion

### 44.4.1 Lithology and Mineralogy of the Sediment Cores

Three short core samples were selected for detailed mineralogical and geochemical analysis, because hydrothermal alteration minerals were dominantly identified by preliminary XRD analysis. Lithological features for the selected three cores (1186MBL, 1188MB, and 1193MB) are given in Table 44.2. Lithological features for other cores are reported in Supplementary file (Suppl. 44.1). Mineral assemblages of the selected three cores determined by XRD analysis are given in Tables 44.3, 44.4, and 44.5, and illustrated in Fig. 44.2. Results of the preliminary XRD analysis for other cores are reported in Supplementary file (Suppl. 44.2).

Mineral assemblages determined by XRD analysis for the two long cores (BMS-J-2 and LC-J-2) are given in Tables 44.6 and 44.7, and illustrated together with visual core description in Figs. 44.3 and 44.4. Sediment core BMS-J-2 can be divided into two units according to the lithology (Fig. 44.3). Unit I (0–380 cmbsf) was silt and clay-sized and olive black colored sediment and contained small-sized pumice (1–10 mm) occasionally. Unit II (380–424 cmbsf) was gray colored sediment which was hydrothermally altered mud and contained granular size of native sulfur crystals occasionally. Sediment core LC-J-2 core can be divided into two units according to the lithology (Fig. 44.4). Unit I (0–300 cmbsf) was silt and clay-sized and olive black colored sediments and contained small-sized pumice (1–10 mm) occasionally. Terrigenous plant debris was observed occasionally between 100–200 cmbsf. Hydrothermally altered pumice was observed at 53, 58, 80, 200, 230, 248 and 250 cmbsf, and native sulfur vein was observed in 25.5, 71.5, 92 and 97 cmbsf. Unit II (300–320 cmbsf) was grayish white colored sediments which was hydrothermal altered mud.

### 44.4.2 Occurrence of Hydrothermal Alteration Minerals in the Surface Sediment Near the High Temperature Fluid Venting Site

The 1186MBL core was collected from the seafloor 50 m distant from the Black Smoker Chimney. The sediment core of 19 cm in length was mostly composed of hydrothermally altered mud. Sulfide minerals and native sulfur grains were commonly observed in 0–17 cmbsf, and a native

**Table 44.3** Mineral assemblage of the short core samples: 1186MBL

| | | Bulk mineralogy | | | | | | | Clay mineralogy | | |
|---|---|---|---|---|---|---|---|---|---|---|---|
| Core ID | Depth (cmbsf) | Q | Pl | Py | Ba | Ga | Sp | S | Sm | Kao | I |
| 1186MBL | 2–4 | XX | | XX | XX | XX | XX | | n.a. | n.a. | n.a. |
| | 4–6 | XX | | XX | XX | XX | XX | | XX | XXX | XX |
| | 6–9 | XX | | | | | | XX | n.a. | n.a. | n.a. |
| | 11–13 | XX | | XX | | | | XX | n.a. | n.a. | n.a. |
| | 15–17 | XX | | XX | | | | XX | XX | XXX | XXX |
| | 17–19 | XX | | XX | | | | XX | n.a. | n.a. | n.a. |
| Sulfur lump collected from 17–19 cmbsf | #1 (black) | XX | XX | | | | | XXX | n.a. | n.a. | n.a. |
| | #2 (gray) | | | | | | | XXX | n.a. | n.a. | n.a. |
| | #3 (gray) | | | | | | | XXX | n.a. | n.a. | n.a. |
| | #4 (gray) | | | | | | | XXX | n.a. | n.a. | n.a. |
| | #5 (gray) | | | | | | | XXX | n.a. | n.a. | n.a. |
| | #6 (yellow) | | | | | | | XXX | n.a. | n.a. | n.a. |

A sulfur lump found in the core at 17–19 cmbsf was divided into six pieces, from #1 (outside) to #6 (inside), and they are provided for XRD analysis
XXX: abundant, XX: common, X: minor
*Q* quartz, *Pl* plagioclase, *Py* pyrite, *Ba* barite, *Ga* galena, *Sp* sphalerite, *S* native sulfur, *Sm* smectite, *Kao* kaolinite, *I* illite
*n.a.* not analyzed

**Table 44.4** Mineral assemblage of the short core samples: 1188MB

| | | Bulk mineralogy | | Clay mineralogy | | |
|---|---|---|---|---|---|---|
| Core ID | Depth (cmbsf) | Q | S | Sm | Chl | I |
| 1188MB | 2–4 | XXX | XX | n.a. | n.a. | n.a. |
| | 6–8 | XXX | XXX | n.a. | n.a. | n.a. |
| | 11–14 | XXX | XXX | XX | XXX | XX |
| | 17–20 | XXX | XXX | n.a. | n.a. | n.a. |

XXX: abundant, XX: common, X: minor
*Q* quartz, *S* native sulfur, *Sm* smectite, *Chl* chlorite, *I* illite
*n.a.* not analyzed

**Table 44.5** Mineral assemblage of the short core samples: 1193MB

| | | Bulk mineralogy | | | | | Clay mineralogy | | |
|---|---|---|---|---|---|---|---|---|---|
| Core ID | Depth (cmbsf) | Q | Pl | Py | Ba | S | Sm | Chl | I |
| 1193MB | 3–5 | XXX | X | XX | XX | XX | n.a. | n.a. | n.a. |
| | 7–9 | XXX | X | XX | XX | XX | XXX | XX | XX |

XXX: abundant, XX: common, X: minor
*Q* quartz, *Pl* plagioclase, *Py* pyrite, *Ba* barite, *S* native sulfur, *Sm* smectite, *Chl* chlorite, *I* illite
*n.a.* not analyzed

sulfur lump of pipe-like shape was found in 17–19 cmbsf. Kaolinite, smectite and illite were identified in the hydrothermally altered mud by XRD analysis (Fig. 44.5a). Quartz, sphalerite, galena, barite and pyrite were identified in 0–6 cmbsf, and quartz, native sulfur and pyrite was identified in 6–17 cmbsf.

Kaolinite is not a common alteration mineral found ubiquitously in seafloor hydrothermal fields. Formation of kaolinite requires acidic environment, but pH buffer potential of seawater would inhibit such environment in the surface sediment. Marumo and Hattori (1999) documented occurrence of kaolinite in the Jade field, and proposed that the surface sediment was associated with acid pore fluids related to oxidation of hydrothermal $H_2S$ to $H_2SO_4$. Indeed, pore fluid of the 1186MBL core showed characteristic low pH (pH = 4.2–4.9) below 6 cmbsf, while the pore fluid above that layer showed pH of seawater level (pH = 7.0–7.6) (Yokoyama et al., Chap. 36). Yokoyama et al. (Chap. 36) proposed that this acidity is related to oxidization and dissolution of sulfide chimney fragments by penetrating seawater rather than oxidation of dissolved $H_2S$. This idea would be supported by observation that the drastic decrease of pore fluid pH below 6 cmbsf corresponds to disappearance of sphalerite and galena both are dominant minerals of sulfide chimneys.

### 44.4.3 Occurrence of Hydrothermal Alteration Minerals in the Surface Sediment Around the Low Temperature Vapor-Rich Fluid Venting Site

The 1188MB core was collected in adjacent to the Biwako Vent. The sediment core of 23 cm in length was mostly composed of white gray colored hydrothermally altered mud. Quartz and native sulfur were identified by XRD analysis of bulk samples, and chlorite, smectite, and illite were identified in the clay fraction (Fig. 44.5b). The 1193MB core was collected from the seafloor where emanation of liquid $CO_2$ bubbling was observed in the vicinity of the Biwako Vent. During ROV return to the sea surface, vigorous bubbling from the corer inside was monitored, which is attributed to decomposition of $CO_2$ hydrate in the sediment as reported by Sakai et al. (1990b). In the sediment core of 11 cm in length, hydrothermally altered mud of

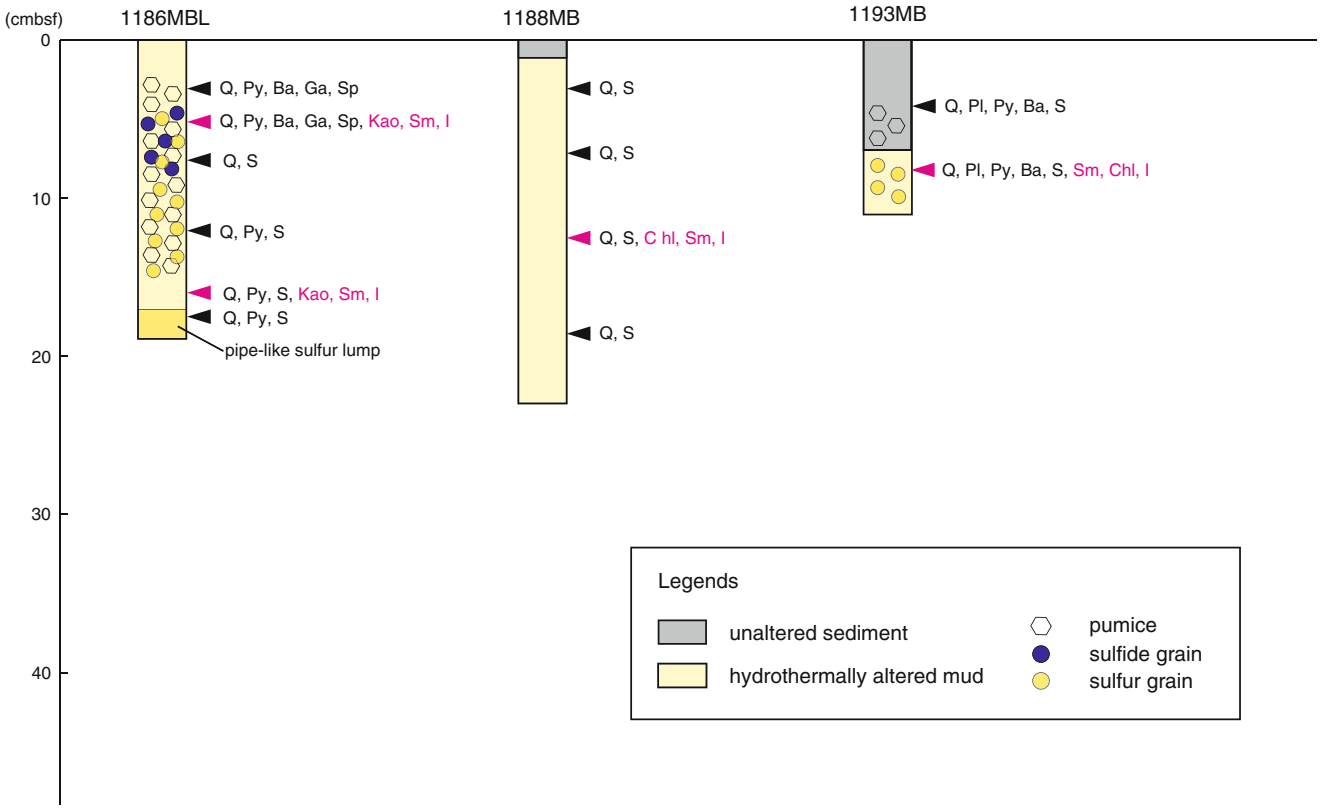


**Fig. 44.2** Visual core description and mineral assemblage of the short cores 1186MBL, 1188MB and 1193MB. Abbreviations for minerals are *Q* quartz, *Pl* plagioclase, *Py* pyrite, *Ba* barite, *Ga* galena, *Sp* sphalerite, *S* native sulfur, *Kao* kaolinite, *Sm* smectite, *I* illite, *Chl* chlorite (Clay minerals are highlighted by *red color text*)

**Table 44.6** Mineral assemblage of the BMS-J-2 core

| | Bulk mineralogy | | | | | Clay mineralogy | | |
|---|---|---|---|---|---|---|---|---|
| Depth (cmbsf) | Q | Cr | Pl | Py | S | Sm | Chl | I |
| 78 | XXX | X | X | | | n.a. | n.a. | n.a. |
| 193.4 | XXX | | X | | | n.a. | n.a. | n.a. |
| 203.9 | XXX | | | | | n.a. | n.a. | n.a. |
| 221.9 | XXX | | | XX | | n.a. | n.a. | n.a. |
| 239.9 | XXX | | X | X | | n.a. | n.a. | n.a. |
| 306.5 | XXX | X | X | | | n.a. | n.a. | n.a. |
| 353.7 | XXX | | | | | n.a. | n.a. | n.a. |
| 363.7 | XXX | X | X | X | | XXX | XX | XX |
| 380.7 | XXX | | | X | | X | XXX | XX |
| 382.7 | XXX | | | | | | | |
| 385.7 | XXX | | | | | X | XXX | XX |
| 390.7 | XXX | | | X | | | | |
| 401.7 | XXX | | | XX | | X | XXX | XX |
| 404.7 | XXX | | | XX | | | | |
| 416.7 | XXX | | | | XX | | XXX | XX |

XXX: abundant, XX: common, X: minor
*Q* quartz, *Cr* cristobalite, *Pl* plagioclase, *Py* pyrite, *S* native sulfur, *Sm* smectite, *Chl* chlorote, *I* illite
*n.a.* not analyzed

whitish color was recognized in 7–9 cmbsf. The hydrothermally altered mud was whitish mud including native sulfur grains. Barite, native sulfur, pyrite, quartz and plagioclase were identified by XRD analysis of bulk samples, and smectite, chlorite and illite were identified in the clay fraction (Fig. 44.5c).

Chemical composition of clay mineral particles from the 1188MB and 1193MB cores was studied by TEM-EDS analysis. Clay mineral particles from the core 1188MR were analyzed together, since a XRD pattern suggesting dominant occurrence of chlorite was recognized during the preliminary analysis. Sampling localities of these three cores were located in close distance less than of 50 m. The TEM-EDS results are presented as a ternary diagram where $Al_2O_3$, MgO and $Fe_2O_3$ ratio is plotted (Fig. 44.6a). Data plots scattered in the region of $Al_2O_3$-rich indicates that Al-rich clay minerals are dominant in these sediment cores. Thus, smectite in these cores is classified as montmorillonite. To examine chemical signature of chlorite in these cores, structural formulae was calculated from the major element chemical composition (Table 44.8a, b). Relative

**Table 44.7** Mineral assemblage of the LC-J-2 core

| | | Bulk mineralogy | | | | | | | | Clay mineralogy | | |
|---|---|---|---|---|---|---|---|---|---|---|---|---|
| Depth (cmbsf) | Description of sample | Q | Cr | Pl | Py | Do | Mag | K | Ap | Sm | Chl | I |
| 40 | Sediment | XXX | | | X | | | | | n.a. | n.a. | n.a. |
| 45 | Pumice | XX | XX | XXX | XX | | | | | n.a. | n.a. | n.a. |
| 50 | Pumice | | XX | XXX | XX | | | | | n.a. | n.a. | n.a. |
| 80 | Hydrothermal altered pumice | XXX | | | | | | | XXX | n.a. | n.a. | n.a. |
| 140 | Sediment | XXX | | | X | | | | | n.a. | n.a. | n.a. |
| 210 | Sediment | XXX | | | X | | | | | n.a. | n.a. | n.a. |
| 248 | Hydrothermal altered pumice | XXX | | | | | | | XXX | n.a. | n.a. | n.a. |
| 260 | Sediment | XXX | | | X | | | | | n.a. | n.a. | n.a. |
| 280 | Sediment | XX | | | | XX | XXX | | | n.a. | n.a. | n.a. |
| 290 | Sediment | XXX | | | X | | X | | | XX | XX | XX |
| CC (upper part) | Grayish white sediment | | | | | | | XXX | | XX | XX | X |
| CC (upper part) | Olive black sediment | XXX | | | | | XX | | | | | |
| CC (lower part) | Grayish white sediment | | | | | | | XXX | | XX | XX | X |
| CC (lower part) | Olive black sediment | XXX | | | | | XX | | | | | |

XXX: abundant, XX: common, X: minor
*Q* quartz, *Cr* cristobalite, *Pl* plagioclase, *Py* pyrite, *Do* dolomite, *Mag* magnesite, *K* K-feldspar, *Ap* apatite, *Sm* smectite, *Chl* chlorote, *I* illite
*n.a.* not analyzed

atomic ratio among Al, Mg and Fe for the chlorite is presented as a ternary diagram (Fig. 44.6b). Chlorite from the 1188B core is Al-rich, while hydrothermal chlorite found in other hydrothermal fields in the Okinawa Trough is characterized as significantly Mg-rich chlorite (Marumo and Hattori (1999) for the Jade field and Miyoshi (2013) for the Iheya North Knoll field). Chemical composition of the chlorite in the 1188MB is close to Al-rich chlorite which is classified as sudoite. Occurrence of sudoite has been reported for only a few examples, where chlorite was associated with other Al-rich clay minerals such as pyrophyllite, kaolinite and diaspora in the outer part of an alteration zone surrounding kuroko-type massive sulfide ore deposit (Inoue and Utada, 1989, Hayashi and Oimura, 1964). Similar zoning of hydrothermal alteration minerals might have developed within the sediment layer in the Jade field.

### 44.4.4 Occurrence of Hydrothermal Alteration Minerals in the Sediment Below the Seafloor Around Active Venting Fluid Sites

The drilled hole for the BMS-J-2 coring operation was confirmed by a ROV dive conducted 3 months after the drilling operation (Ishibashi et al., Chap. 31), which was located ~50 m south of the Biwako Vent. Somehow different mineral assemblages were recognized between in Unit I and II (Table 44.6 and Fig. 44.3). Quartz was dominantly found through Units I to II. Cristobalite and plagioclase were found occasionally in Unit I, but were not found in Unit II. Pyrite was found occasionally in Units I and II. Clay mineralogy of sediments from 364 cmbsf (Unit I) and 381–417 cmbsf (Unit II) was examined by XRD analysis. Smectite, chlorite and illite were identified in 364 cmbsf (Unit I) (Fig. 44.7a). Chlorite and illite were mainly identified in 381–417 cmbsf (Unit II) (Fig. 44.7b, c).

A locality of the LC-J-2 coring site is estimated as very close to the Biwako vent, although it could not be determined accurately because the coring operation was conducted during a surface ship cruise. Intense hydrothermal alteration was recognized only in Unit II (Table 44.7 and Fig. 44.4). Quartz was dominantly found in Unit I. Pyrite was found in Unit I occasionally. In the lower depth (280–300 cmbsf) of Unit I, carbonate minerals, dolomite and magnesite, were recognized. Quartz, cristobalite, plagioclase and pyrite were dominantly identified in pumice grains at 45 and 50 cmbsf in Unit I. A large broad peak around $2\theta = 20–30°$ in the XRD patterns of the grains was also recognized indicating presence of large amounts of volcanic glass. Apatite and quartz were identified in grains of hydrothermal altered pumice at 80 and 248 cmbsf in Unit I (Fig. 44.8a). Abundant K-feldspar was identified in grayish white sediment samples in Unit II (Fig. 44.8b). Quartz and magnesite were found in olive black sediment samples in Unit II. Clay mineralogy was examined for sediments from 290 cmbsf (Unit I) and 300–330 cmbsf (Unit II). Smectite, chlorite and illite were identified at 290 cmbsf (Unit I). Smectite, chlorite and illite were found at 300–330 cmbsf (Unit II) (Fig. 44.8 c).

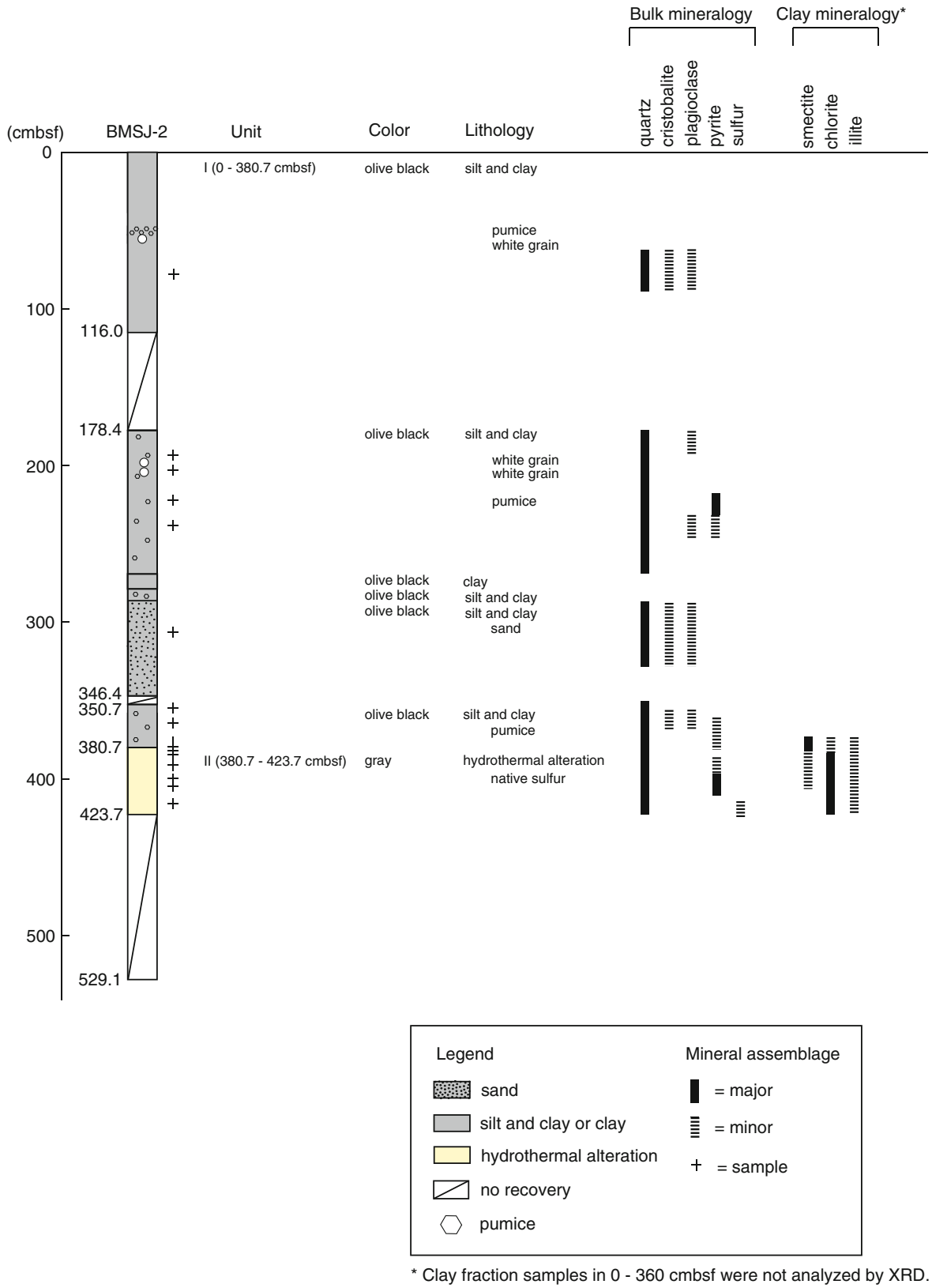


**Fig. 44.3** Visual core description and mineral assemblage of the BMS-J-2 core; cmbsf is abbreviation for centimeters below seafloor. The *cross marks* indicate the depths of the samples analyzed in this study. The *bold* and *dashed lines* indicate distribution of main and minor minerals. *Clay fraction samples in 0–360 cmbsf were not analyzed by XRD

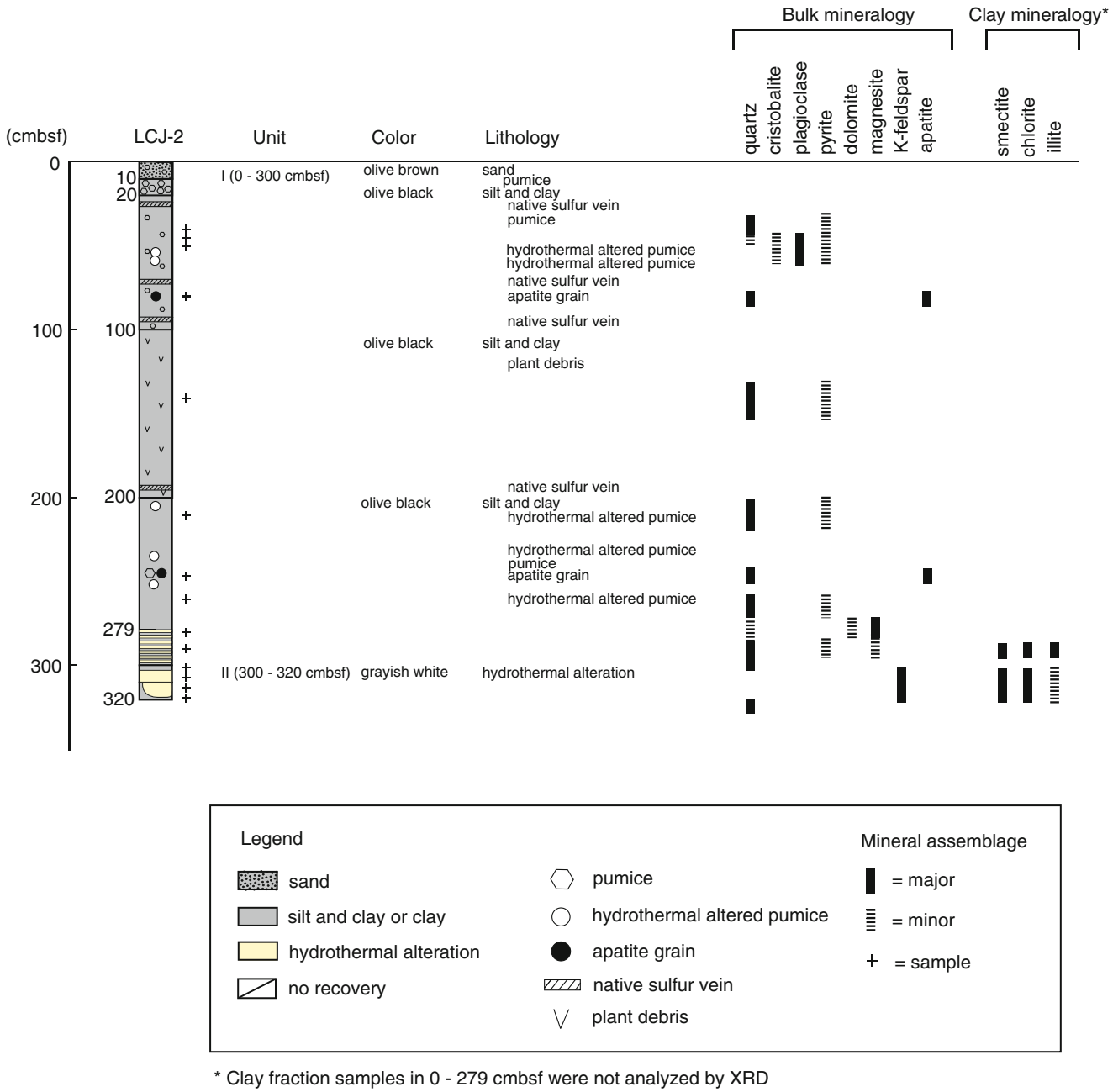


**Fig. 44.4** Visual core description and mineral assemblage of the LC-J-2 core; cmbsf is abbreviation for centimeters below seafloor. The *crosses* indicate the depths of the samples analyzed in this study. The *bold* and *dashed lines* indicate distribution of main and minor minerals. *Clay fraction samples in 0–279 cmbsf were not analyzed by XRD

Detailed chemical analysis using EPMA was conducted for specific minerals such as apatite and K-feldspar identified in the LC-J-2 core. Back-scattered electron (BSE) images of the hydrothermal altered pumice where apatite was identified (at 80 cmbsf and 248 cmbsf, Unit I) are shown in Fig. 44.9. Apatite was observed as associated with clay minerals and pyrite (Fig. 44.9a, b). In addition to apatite, monazite was identified as bright white crystals (Fig. 44.9c), which was associated with rutile, pyrite and clay minerals. Determined chemical compositions of the apatite and monazite are given in Table 44.9. The apatite contained minor amounts of REEs (Rare earth elements) and fluorine, and the monazite was more enriched in REE. BSE images of the grayish white sediment where K-feldspar was identified (300–330 cmbsf, Unit II) are shown in Fig. 44.10. Euhedral crystals of K-feldspar in size up to several tens μm

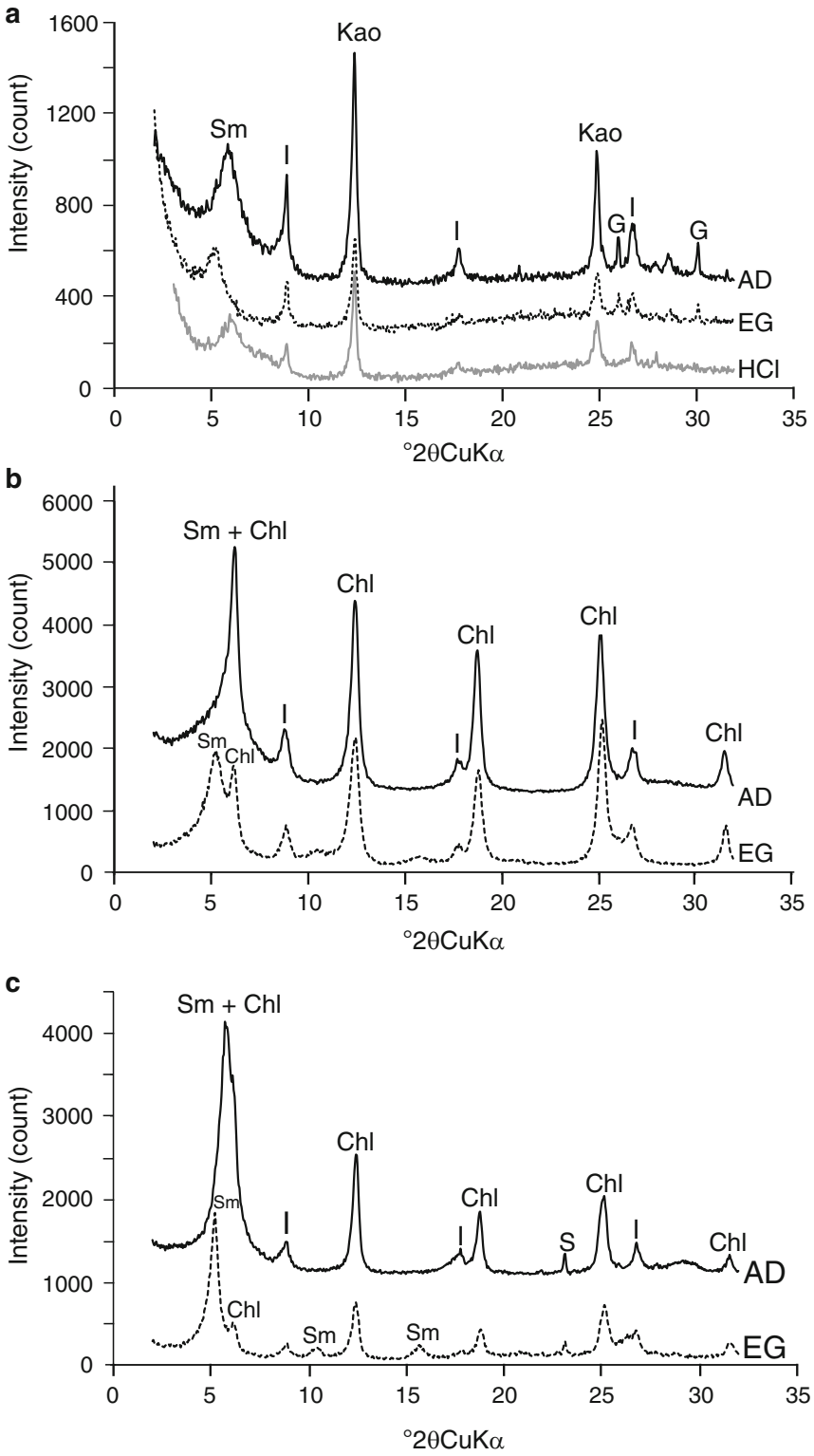


**Fig. 44.5** XRD patterns of clay fractions seprated from the samples (**a**) 1186MBL 4–6 cmbsf, (**b**) 1188MB 11–14 cmbsf, and (**c**) 1193MB 7–9 cmbsf. Abbreviations for minerals are *Kao* kaolinite, *Sm* smectite, *Chl* chlorite, *I* illite, *G* galena, *S* native sulfur. The *solid line* (AD), the *dashed line* (EG), and the *gray line* (HCl) indicated XRD patterns of air-dried sample, of ethylene glycol saturated sample, and of HCl treated sample, respectively

were recognized among clay minerals. Off-white portion of the K-feldspar crystals (analytical points #2, #3 and #7 in Fig. 44.10) showed slightly high BaO concentration (BaO = 1.1–2.5 wt%, Table 44.10). Based on the EPMA analysis, clay minerals of feather-like morphology (analytical point #4 in Fig. 44.10) contains Mg, while clay minerals of layer stack morphology (analytical points #6 and #9 in Fig. 44.10) lacks Mg and composed of only Al and Si.

K-feldspar is known as formed by high temperature hydrothermal alteration (Yoshimura, 2001). The observed

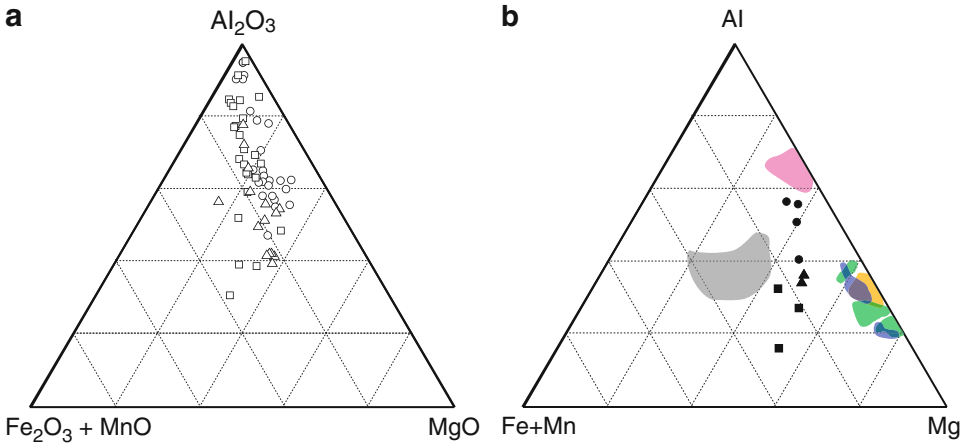


**Fig. 44.6** Chemical composition of clay minerals in three short cores collected from near the Biwako Vent. (**a**) $Al_2O_3$, MgO and $Fe_2O_3$ ratio of the clay fraction samples, 1188MB 11–14 cmbsf (*open circle*), 1193MB 7–9 cmbsf (*open square*), and 1188MR 4–6 cmbsf (*open triangle*). (**b**) Al, Mg and Fe atomic ratio of chlorite in clay fraction samples, 1188MB 11–14 cmbsf (*solid circle*), 1193MB 7–9 cmbsf (*solid square*), and 1188MR 4–6 cmbsf (*solid triangle*). The *color shaded areas* represent range of chemical composition of chlorite recognized in alteration zones in seafloor hydrothermal fields and around kuroko-type ore deposit. *Orange*: hydrothermal chlorite from the Jade field (Marumo and Hattori, 1999). *Gray*: detrital chlorite from the Izena Hole (Marumo and Hattori, 1999). *Green*: chlorite and chlorite-smectite mixed-layer mineral from the Iheya North Knoll field in the Okinawa Trough (Miyoshi, 2013). *Pink*: sudoite (Al-rich chlorite) from Kamikita mine, Aomori Prefecture, Japan (Inoue and Utada, 1989). *Blue*: Mg-rich chlorite and chlorite-smectite mixed-layer mineral from Furutobe and Hanaoka mines, Akita Prefecture, and Wanibuchi and Iwami mines, Shimane Prefecture, Japan (Shirozu et al., 1975)

**Table 44.8** Results of TEM-EDS analysis for chlorite particles separated from cores collected from in the vicinity of the Biwako Vent

| Core ID | 1188MB | 1188MB | 1188MB | 1188MB | 1193MB | 1193MB | 1193MB | 1188MR | 1188MR |
|---|---|---|---|---|---|---|---|---|---|
| Depth (cmbsf) | 11–14 | 11–14 | 11–14 | 11–14 | 7–9 | 7–9 | 7–9 | 4–6 | 4–6 |
| Mineral | Chl | Chl | Chl | Chl | Chl | Chl | Chl | Chl | Chl |
| (a) Major element composition of chlorite | | | | | | | | | |
| Element (wt%) | | | | | | | | | |
| $SiO_2$ | 43.8 | 46.4 | 45.0 | 42.4 | 40.1 | 35.9 | 31.5 | 44.0 | 42.0 |
| $TiO_2$ | n.d. | n.d. | n.d. | n.d. | n.d. | n.d. | n.d. | n.d. | n.d. |
| $Al_2O_3$ | 32.0 | 32.6 | 34.0 | 27.2 | 23.4 | 24.7 | 20.8 | 23.5 | 24.2 |
| $Fe_2O_3$ | 7.81 | 7.11 | 5.49 | 11.7 | 18.7 | 17.5 | 25.8 | 12.4 | 13.5 |
| MgO | 16.4 | 13.9 | 15.4 | 18.8 | 17.9 | 22.0 | 22.0 | 20.1 | 20.4 |
| MnO | n.d. | n.d. | n.d. | n.d. | n.d. | n.d. | n.d. | n.d. | n.d. |
| CaO | n.d. | n.d. | n.d. | n.d. | n.d. | n.d. | n.d. | n.d. | n.d. |
| $Na_2O$ | n.d. | n.d. | n.d. | n.d. | n.d. | n.d. | n.d. | n.d. | n.d. |
| $K_2O$ | n.d. | n.d. | n.d. | n.d. | n.d. | n.d. | n.d. | n.d. | n.d. |
| Total | 100 | 100 | 100 | 100 | 100 | 100 | 100 | 100 | 100 |
| (b) Calculated structural formulae of chlorite: on the basis of $O_{10}(OH)_8$ | | | | | | | | | |
| *Tetrahedral* | | | | | | | | | |
| Si | 3.46 | 3.63 | 3.51 | 3.41 | 3.32 | 2.99 | 2.73 | 3.55 | 3.41 |
| Al | 0.54 | 0.37 | 0.49 | 0.59 | 0.68 | 1.01 | 1.27 | 0.45 | 0.59 |
| Sum | 4.00 | 4.00 | 4.00 | 4.00 | 4.00 | 4.00 | 4.00 | 4.00 | 4.00 |
| *Octahedral* | | | | | | | | | |
| Al | 2.43 | 2.63 | 2.64 | 1.99 | 1.60 | 1.42 | 0.85 | 1.78 | 1.73 |
| Fe(3+) | 0.46 | 0.42 | 0.32 | 0.71 | 1.16 | 1.10 | 1.68 | 0.75 | 0.82 |
| Mg | 1.93 | 1.61 | 1.79 | 2.25 | 2.20 | 2.73 | 2.84 | 2.42 | 2.47 |
| Total | 4.82 | 4.66 | 4.76 | 4.95 | 4.96 | 5.25 | 5.37 | 4.95 | 5.02 |

*Chl* chlorite
*n.d.* not detected
Total Fe was expressed as $Fe_2O_3$

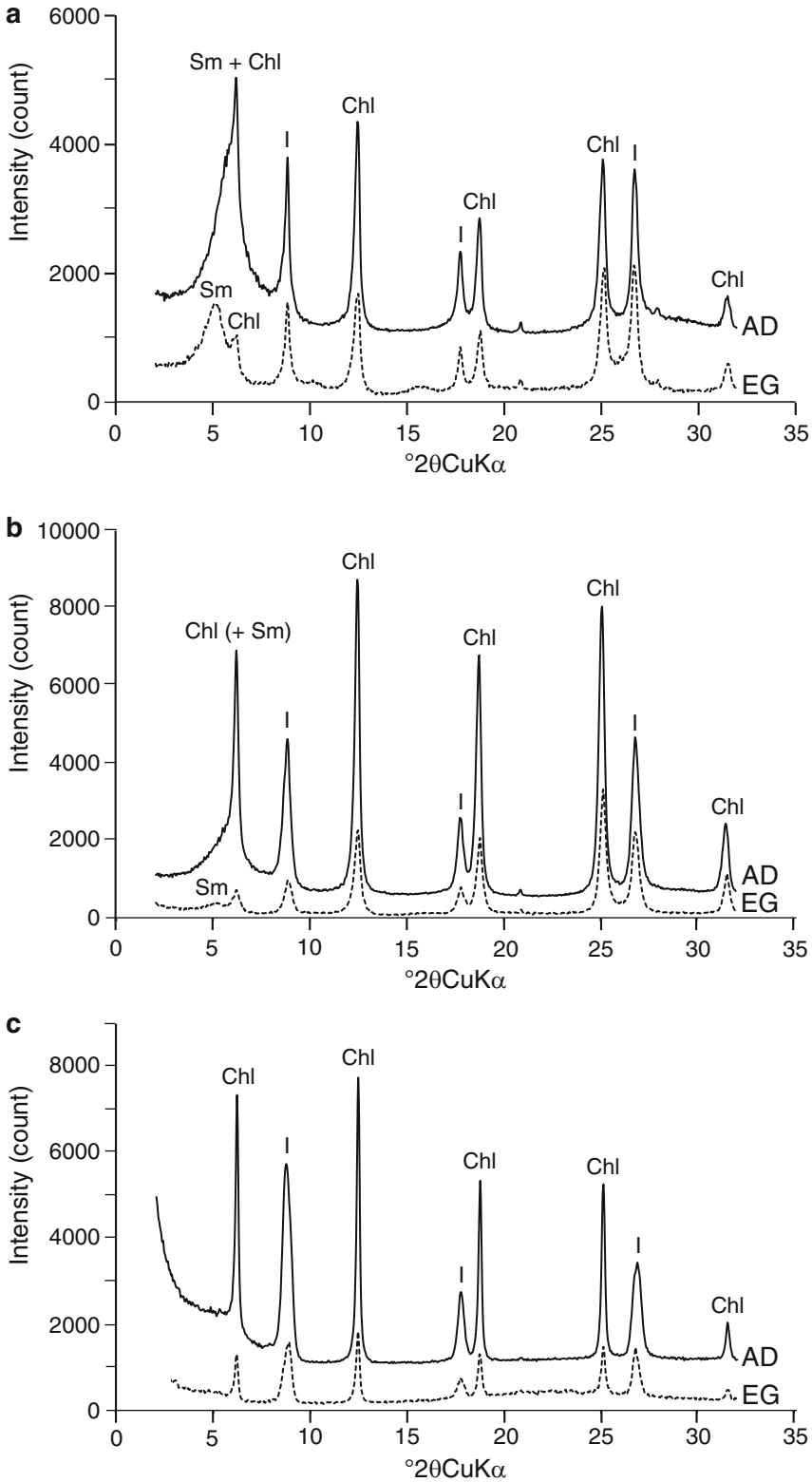


**Fig. 44.7** XRD patterns of clay fractions seprated from the BMS-J-2 core at (**a**) 363.7 cmbsf, (**b**) 380.7 cmbsf and (**c**) 416.7 cmbsf. Abbreviations for minerals are *Sm* smectite, *Chl* chlorite, *I* illite. The *solid line* (AD) and *dashed line* (EG) indicate XRD patterns of air-dried samples and ethylene glycol saturated samples

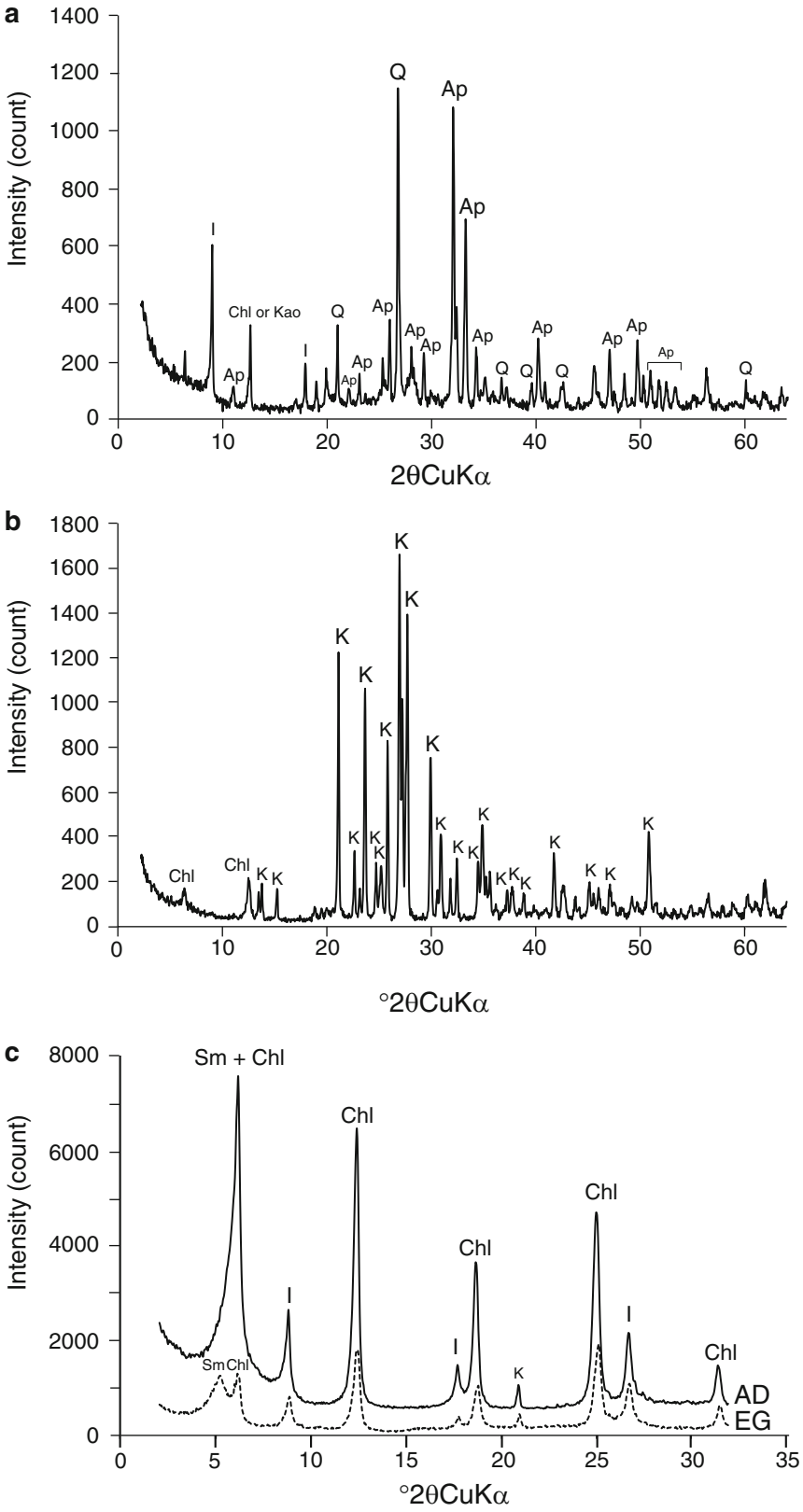


**Fig. 44.8** XRD patterns of sediment from the LC-J-2 core, (**a**) hydrothermal altered pumice at 248 cmbsf, (**b**) grayish white sediment from CC (lower part), (**c**) clay fraction of the same sediment as (**b**). Abbreviations for minerals are *Q* quartz, *Ap* apatite, *I* illite, *Chl* chlorite, *Kao* kaolinite, *K* F-feldspar, *Sm* smectite. The *solid line* (AD) and *dashed line* (EG) indicate XRD patterns of air-dried samples and ethylene glycol saturated samples

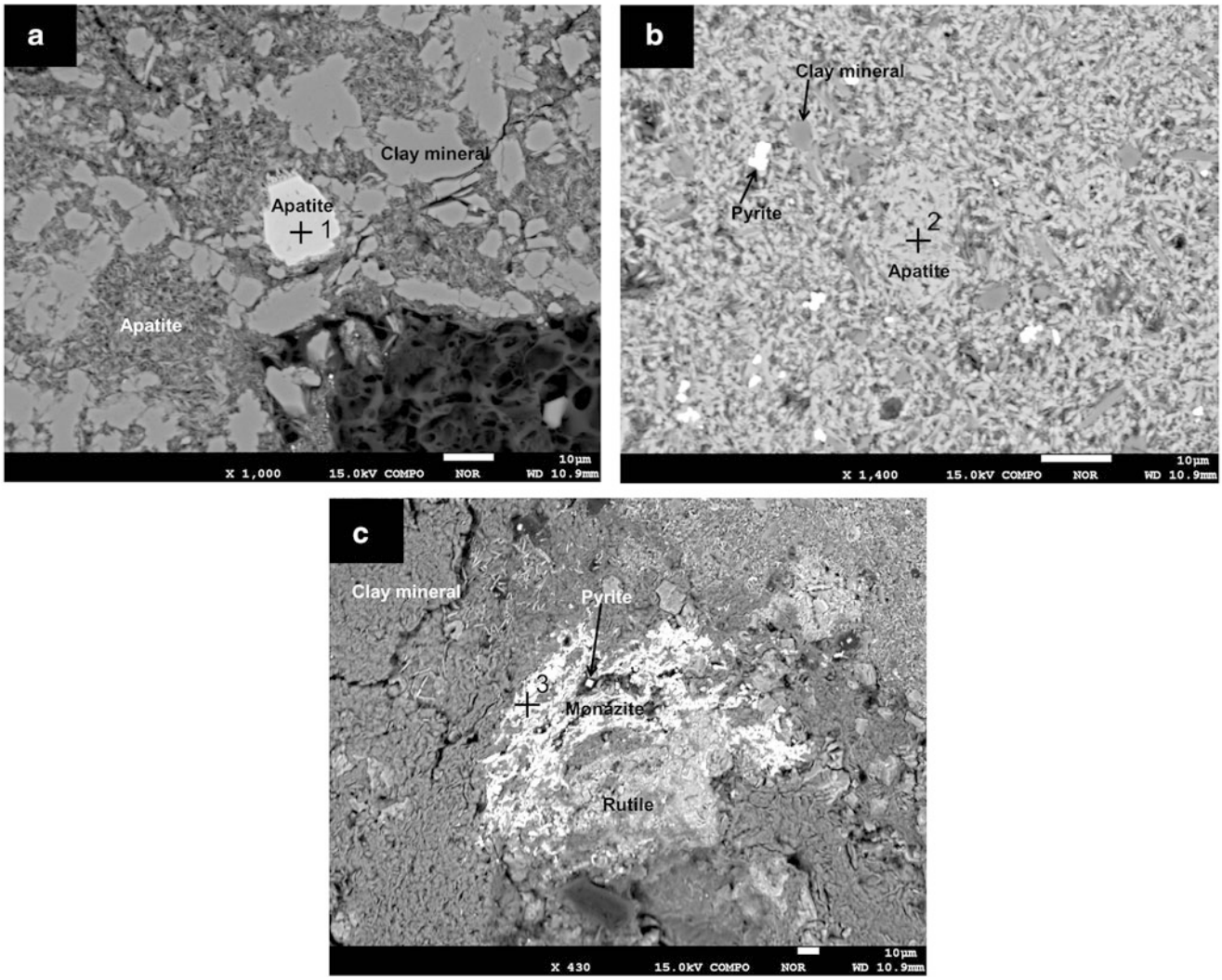


**Fig. 44.9** Back-scattered electron (BSE) images obtained by EPMA analysis of hydrothermal altered pumice found in the LC-J-2 core at (**a**) 80 cmbsf, (**b**) 248 cmbsf, and (**c**) 248 cmbsf. The *cross marks* indicate points for determination of chemical composition, which results are listed in Table 44.9

**Table 44.9** Results of EPMA analysis for specific minerals in the hydrothermal altered pumice at 80 and 240 cmbsf in the LC-J-2 core

| Analyzed point[a] | 1 | 2 | 3 |
|---|---|---|---|
| Mineral | Apatite | Apatite | Monazite |
| Element (wt%) | | | |
| CaO | 54.4 | 48.1 | 5.30 |
| $Y_2O_3$ | 0.24 | 0.03 | 0.64 |
| $La_2O_3$ | n.d. | 0.03 | 8.16 |
| $Ce_2O_3$ | 0.14 | 0.18 | 23.0 |
| $Pr_2O_3$ | 0.22 | 0.01 | 4.55 |
| $Nd_2O_3$ | 0.33 | n.d. | 9.02 |
| $Sm_2O_3$ | 0.07 | n.d. | 1.42 |
| $Gd_2O_3$ | 0.13 | 0.08 | 2.83 |
| $ThO_2$ | 0.08 | n.d. | 0.22 |
| $UO_2$ | 0.07 | 0.02 | 0.01 |
| $P_2O_5$ | 43.4 | 34.3 | 21.7 |
| F | 3.88 | 4.57 | 0.53 |
| Total | 101 | 85.4 | 77.2 |
| ΣREE | 1.13 | 0.33 | 49.6 |
| ΣLREE | 0.76 | 0.22 | 46.2 |
| ΣHREE | 0.13 | 0.08 | 2.83 |

[a]Numbers of analyzed points correspond to those of cross points in Fig. 44.9
*n.d.* not detected

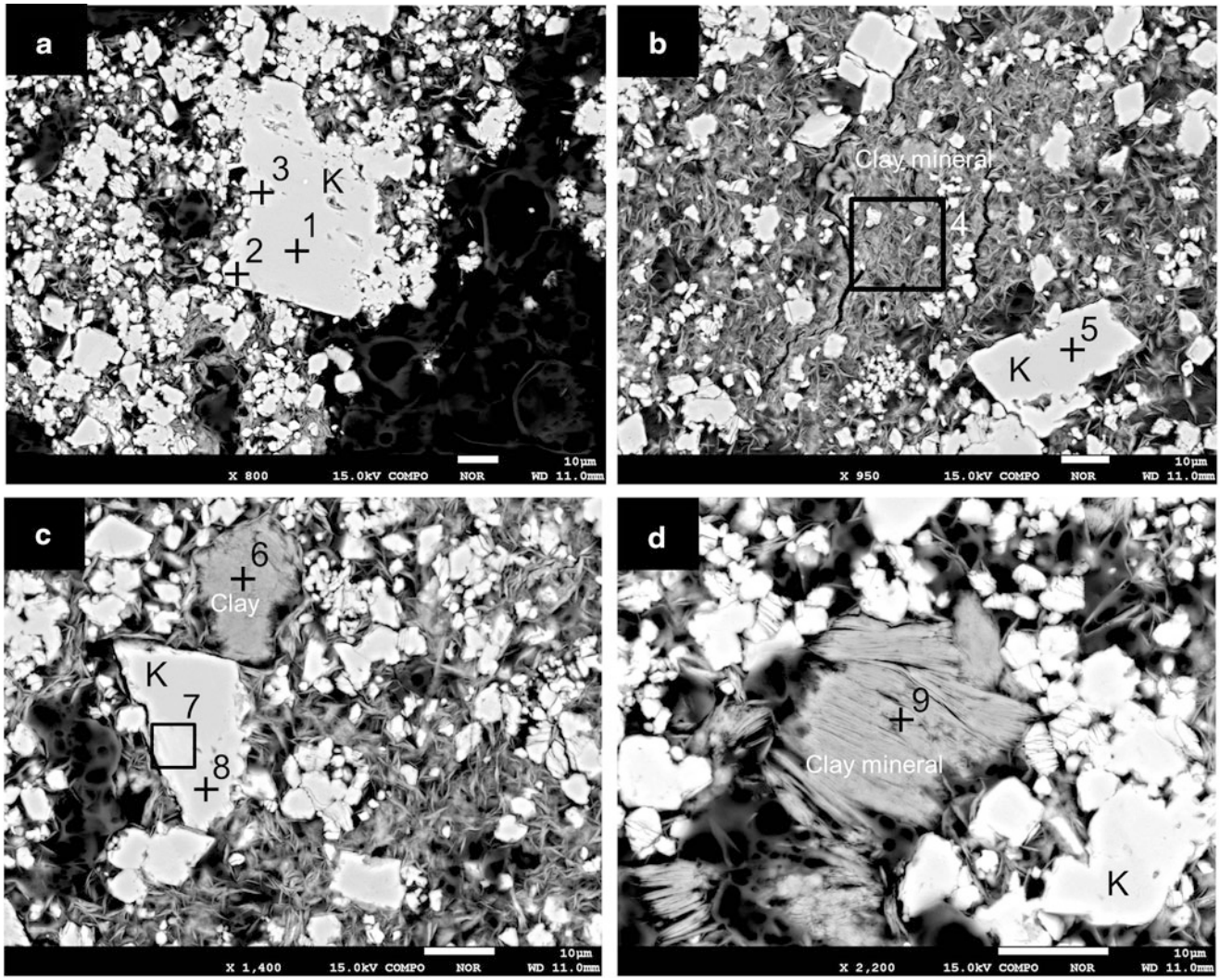


**Fig. 44.10** Back-scattered electron (BSE) images obtained by EPMA analysis of the grayish white sediment found in CC (core catcher) of the LC-J-2 core. The *cross marks* indicate points for determination of chemical composition, which results are listed in Table 44.10

**Table 44.10** Results of EPMA analysis for specific minerals in the grayish white sediment at CC (core catcher) in the LC-J-2 core

| Analyzed point[a] | 1 | 2 | 3 | 4 | 5 | 6 | 7 | 8 | 9 |
|---|---|---|---|---|---|---|---|---|---|
| Mineral | K-feldspar | K-feldspar (Ba-rich) | K-feldspar (Ba-rich) | Feather-like clay | K-feldspar | Layer stack clay | K-feldspar (Ba-rich) | K-feldspar | Layer stack clay |
| Element (wt%) | | | | | | | | | |
| $SiO_2$ | 66.3 | 63.4 | 63.8 | 29.9 | 66.2 | 46.4 | 64.8 | 64.3 | 47.0 |
| $TiO_2$ | n.d. | 0.68 | 0.57 | 0.32 | n.d. | 0.02 | 0.43 | 0.01 | 0.04 |
| $Al_2O_3$ | 17.9 | 18.5 | 18.7 | 16.8 | 17.5 | 37.0 | 18.3 | 17.7 | 38.1 |
| FeO | n.d. | 0.01 | n.d. | 1.64 | n.d. | 0.01 | n.d. | 0.07 | 0.13 |
| MnO | 0.01 | n.d. | n.d. | 0.13 | 0.05 | 0.04 | n.d. | 0.07 | n.d. |
| MgO | n.d. | 0.10 | n.d. | 16.8 | 0.03 | 0.37 | n.d. | 0.06 | 0.59 |
| CaO | n.d. | 0.05 | 0.03 | 0.50 | n.d. | 0.11 | n.d. | n.d. | 0.21 |
| $Na_2O$ | 0.32 | 0.30 | 0.25 | 0.10 | 0.11 | 0.08 | 0.24 | 0.21 | 0.04 |
| $K_2O$ | 16.1 | 15.5 | 15.6 | 0.25 | 14.7 | 1.76 | 14.1 | 15.8 | 0.10 |
| BaO | 0.16 | 1.09 | 2.36 | n.d. | n.d. | 0.31 | 2.48 | n.d. | n.d. |
| SrO | 0.35 | 0.35 | 0.45 | 0.13 | 0.18 | 0.55 | 0.37 | 0.54 | 0.20 |
| $SO_3$ | n.d. | n.d. | n.d. | 0.18 | n.d. | 0.16 | n.d. | n.d. | n.d. |
| Total | 101 | 100 | 102 | 66.8 | 98.8 | 86.7 | 101 | 98.8 | 86.5 |

[a]Numbers of analyzed points correspond to those of cross points and square areas in Fig. 44.10
*n.d.* not detected

occurrence as euhedral crystal grown up to larger than 10 μm suggests formation by precipitation from high temperature fluid. Alteration mineral assemblages included K-feldspar were reported for the core obtained by ODP (ocean drilling project) seafloor drilling in the Pacmanus hydrothermal field, the Manus Basin (Paulick and Bach, 2006). They documented chlorite-illite-K-feldspar assemblages accompanied by quartz, smectite, and pyrite in the core below 25 mbsf obtained by drilling immediately adjacent to a high-temperature vent. They suggested that the high temperature alteration is related to sulfide mineralization in a stockwork zone. The alteration mineral assemblage recognized in the Unit II of LC-J-2 core is similar to that found in the Pacmanus hydrothermal field, although the sediment was obtained only 3 mbsf. The hydrothermal mineral assemblage found in this study implies sulfide mineralization below the seafloor around the Biwako Vent, in spite of no evidence on the seafloor.

**Acknowledgement** We are grateful to the team members of ROV Hyper-Dolphin, crew of R/V Natsushima and onboard scientists during NT10-17 cruise. We are grateful to the team members of the Benthic Multi-coring System (BMS), the crew of the R/V Hakurei-maru No. 2, and onboard scientists during TAIGA11 cruise. We thank the Research Laboratory for High Voltage Electron Microscopy at Kyushu University for their support for TEM analysis. We are grateful to Associate Professor Kyoko Okino of the University of Tokyo, who hosted the first author (Y. M.)'s stay in the Atmosphere and Ocean Research Institute by T-MORE program (TAIGA Mentorship On Research and Education). This article is a part of the doctoral thesis of the first author (Y. M.). We thank Professor Tasuku Akagi of Kyushu University and Professor Harue Masuda of Osaka City University for their insightful advice. This study was supported by a Scholarship for Ph.D. candidates of the Faculty of Sciences, Kyushu University (to the first author (Y. M.)). This study was also partly supported by the "TAIGA project" which was funded by a Grant-in-Aid for Scientific Research on Innovative Areas (#20109004) from the Ministry of Education, Culture, Sports, Science and Technology (MEXT), Japan.



## References

Hayashi H, Oimura K (1964) Aluminian chlorite from Kamikita mine, Japan. Clay Sci 2(1):22–30

Inoue A, Utada M (1989) Mineralogy and genesis of hydrothermal aluminous clays containing sudoite, tosudite, and rectorite in a drillhole near the Kamikita Kuroko ore deposit, northern Honshu, Japan. Clay Sci 7:193–217

Ishibashi J, Noguchi T, Toki T, Miyabe S, Yamagami S, Onishi Y, Yamanaka T, Yokoyama Y, Omori E, Takahashi Y, Hatada K, Nakaguchi Y, Yoshizaki M, Konno U, Shibuya T, Takai K, Inagaki F, Kawagucci S (2014) Diversity of fluid geochemistry affected by processes during fluid upwelling in active hydrothermal fields in the Izena Hole, the middle Okinawa Trough back-arc basin. Geochem J 48(3):357–369

Marumo K, Hattori K (1999) Seafloor hydrothermal clay alteration at Jade in the back-arc Okinawa Trough: mineralogy, geochemistry and isotope characteristics. Geochim Cosmochim Acta 63 (18):2785–2804

Miyoshi Y (2013) Mineralogical and geochemical studies of hydrothermal clay minerals below the seafloor at active hydrothermal fields in the island arc and back-arc setting, doctoral thesis in Kyushu University, Japan

Paulick H, Bach W (2006) Phyllosilicate alteration mineral assemblages in the active subsea-floor Pacmanus hydrothermal system, Papua New Guinea, ODP Leg 193. Econ Geol 101:633–650

Sakai H, Gamo T, Kim E-S, Shitashima K, Yanagisawa F, Tsutsumi M, Ishibashi J, Sano Y, Wakita H, Tanaka T, Matsumoto T, Naganuma T, Mitsuzawa K (1990a) Unique chemistry of the hydrothermal solution in the mid-Okinawa Trough backarc basin. Geophys Res Lett 17(12):2133–2136

Sakai H, Gamo T, Kim ES, Tsutsumi M, Tanaka T, Ishibahi J, Wakita H, Yamano M, Oomori T (1990b) Venting of carbon dioxide-rich fluid and hydrate formation in mid-Okinawa Trough Backarc Basin. Science 248:1093–1096

Shirozu H, Sakasegawa T, Katsumoto N (1975) Mg-chlorite and interstratified Mg-chlorite/saponite associated with Kuroko deposits. Clay Sci 4:305–321

Takai K, Mottl MJ, Nielsen SH, The IODP Expedition 331 Scientists (2011) Proceedings of the integrated ocean drilling program, vol 331. Integrated Ocean Drilling Program Management International, Tokyo

Yoshimura (2001) Clay minerals and alterations. The Association for the geological collaboration in Japan (AGCJ), in Japanese